The X-Shooter Lens Survey - I. Dark matter domination and a Salpeter-type initial mass function in a massive early-type galaxy

Spiniello, C.; Koopmans, L. V. E.; Trager, S. C.; Czoske, O.; Treu, T.

Published in:
Monthly Notices of the Royal Astronomical Society

DOI:
10.1111/j.1365-2966.2011.19458.x

Publication date:
2011

Monthly Notices
of the
ROYAL ASTRONOMICAL SOCIETY

Mon. Not. R. Astron. Soc. **417,** 3000–3009 (2011) doi:10.1111/j.1365-2966.2011.19458.x

The X-Shooter Lens Survey – I. Dark matter domination and a Salpeter-type initial mass function in a massive early-type galaxy

C. Spiniello,[1⋆] L. V. E. Koopmans,[1] S. C. Trager,[1] O. Czoske[2] and T. Treu[3]

[1]*Kapteyn Institute, University of Groningen, PO Box 800, 9700 AV Groningen, the Netherlands*
[2]*Institut für Astronomie, Universität Wien, Türkenschanzstraβe 17, 1180 Wien, Austria*
[3]*Department of Physics, University of California Santa Barbara, Santa Barbara, CA 93106, USA*

Accepted 2011 July 15. Received 2011 June 21; in original form 2011 March 23

ABSTRACT

We present the first results from the X-Shooter Lens Survey: an analysis of the massive early-type galaxy SDSS J1148+1930 at redshift $z = 0.444$. We combine its extended kinematic profile – derived from spectra obtained with X-Shooter on the European Southern Observatory Very Large Telescope – with strong gravitational lensing and multicolour information derived from Sloan Digital Sky Survey (SDSS) images. Our main results are as follows. (i) The luminosity-weighted stellar velocity dispersion is $\langle\sigma_*\rangle(\lesssim R_{\rm eff}) = 352 \pm 10 \pm 16\,{\rm km\,s^{-1}}$, extracted from a rectangular aperture of $1.8 \times 1.6\,{\rm arcsec}^2$ centred on the galaxy, more accurate and considerably lower than a previously published value of $\sim$450 km s^{-1}. (ii) A single-component (stellar plus dark) mass model of the lens galaxy yields a logarithmic total-density slope of $\gamma' = 1.72^{+0.05}_{-0.06}$ (68 per cent confidence level, CL; $\rho_{\rm tot} \propto r^{-\gamma'}$) within a projected radius of $\sim$2.16 arcsec. (iii) The projected stellar mass fraction, derived solely from the lensing and dynamical data, is $f_*(<R_{\rm E}) = 0.19^{+0.04}_{-0.09}$ (68 per cent CL) inside the Einstein radius for a Hernquist stellar profile and no anisotropy. The dark matter fraction inside the effective radius $f_{\rm DM}(<R_{\rm eff}) = 0.60^{+0.15}_{-0.06} \pm 0.1$ (68 per cent CL), where the latter error is systematic. (iv) Based on the SDSS colours, we find $f_{*,\rm Salp}(<{\rm R_E}) = 0.17 \pm 0.06$ for a Salpeter initial mass function (IMF) and $f_{*,\rm Chab}(<{\rm R_E}) = 0.07 \pm 0.02$ for a Chabrier IMF. The lensing and dynamics constraints on the stellar mass fraction agree well with those independently derived from the SDSS colours for a Salpeter IMF, which is preferred over a Chabrier IMF at variance with standard results for lower mass galaxies. Dwarf-rich IMFs in the lower mass range of 0.1–0.7 $\rm M_\odot$, with $\alpha \geq 3$ (with ${\rm d}N/{\rm d}M \propto M^{-\alpha}$) – such as that recently suggested for massive early-type galaxies with $\alpha = 3$ in the mass range 0.1–1 $\rm M_\odot$ – are excluded at the >90 per cent CL and in some cases violate the total lensing-derived mass limit. We conclude that this very massive early-type galaxy is dark-matter-dominated inside one effective radius, consistent with the trend recently found from massive Sloan Lens ACS (SLACS) galaxies, with a total density slope shallower than isothermal and an IMF normalization consistent with Salpeter.

Key words: gravitational lensing: strong – galaxies: elliptical and lenticular, cD – galaxies: formation – galaxies: kinematics and dynamics – galaxies: structure – dark matter.

1 INTRODUCTION

Understanding the evolution and the internal structure of massive early-type galaxies (ETGs), as well as their stellar and dark matter (DM) distributions, is crucial in order to fully comprehend the processes in hierarchical galaxy formation (e.g. White & Rees 1978; Davis et al. 1985; Frenk 1985). In this context, the relationship between baryonic matter, which dominates astrophysical observables, and DM, which dominates most of the dynamics during galaxy formation, is particularly important.

To unravel some of these issues and paint a more robust physical picture, enormous effort has been afforded to study the relative contributions of baryonic, DM and black hole constituents of ETGs through stellar dynamical tracers, X-ray studies and gravitational lensing (e.g. Fabbiano 1989; Mould et al. 1990; Saglia, Bertin & Stiavelli 1992; Bertin et al. 1994; Franx, van Gorkom & de Zeeuw 1994; Carollo et al. 1995; Arnaboldi et al. 1996; Rix et al. 1997; Matsushita et al. 1998; Loewenstein & White 1999; Gerhard et al. 2001; Seljak 2002; Borriello, Salucci & Danese 2003; Romanowsky

⋆E-mail: spiniello@astro.rug.nl

et al. 2003; Cappellari & Emsellem 2004; Treu & Koopmans 2004; Cappellari et al. 2006; Treu et al. 2006; Thomas et al. 2007; Czoske et al. 2008; Auger et al. 2010a,b; Treu 2010).

The picture emerging over the last decades from studies of the inner regions of ETGs, where baryonic and DM are both present, is that to first order the total mass density profile inside few effective radii can be well described by a power-law form close to an isothermal profile with $\gamma \approx 2$ for $\rho_{\rm tot} = r^{-\gamma'}$, although with a $\sim$10 per cent intrinsic scatter in the density profile (e.g. Gerhard et al. 2001; Treu & Koopmans 2004; Koopmans et al. 2006, 2009; Barnabé et al. 2009, 2011; Auger et al. 2010a). The DM density profile in the same region, however, is far less well constrained, although seems consistent with a density slope $\gamma_{\rm DM} \approx 1.3$ (e.g. Treu & Koopmans 2004).

In addition, while the innermost regions of ETGs are expected to be dominated by the stellar mass component, the DM mass component is usually found to play a non-negligible role, with mass fractions ranging from 10 to 40 per cent of the total mass within one effective radius (e.g. Gerhard et al. 2001; Cappellari et al. 2006; Gavazzi et al. 2007; Weijmans et al. 2008). Even more recently, observations, as well as theoretical studies based on stellar population and dynamical models (e.g. Bullock et al. 2001; Padmanabhan et al. 2004), indicate that, for a constant initial mass function (IMF), the DM fraction in the internal region increases monotonically with the mass of the galaxy (e.g. Zaritsky, Gonzalez & Zabludoff 2006; Auger et al. 2010b), a trend that is more conspicuous in the case of slow-rotator ellipticals (Tortora et al. 2009). On the other hand, it has also been shown that the luminous stellar mass-to-light (M/L) ratio scales with the luminous mass of the system (Grillo et al. 2009). However, information from stellar kinematics is limited to the central regions (a few effective radii) because of the lack of bright kinematic tracers at large radii, and the total mass determination suffers from the well-known degeneracy between the mass density profile of the galaxy and the anisotropy of its stellar velocity dispersion tensor (Binney & Mamon 1982). Higher order velocity moments, which potentially allow one to disentangle this degeneracy by providing additional constraints (Gerhard 1993; van der Marel & Franx 1993), can only be measured with sufficient accuracy in the inner parts of nearby galaxies with current instruments. Despite great progress, it still remains difficult to separate the stellar and DM components, mostly due to a still relatively poor understanding of the precise shape of the stellar IMF and its associated stellar M/L ratio. Uncertainties related to the latter can easily lead to a factor of a few uncertainty in the inferred stellar mass.

Understanding the stellar IMF in massive ETGs is a key open issue with a broad range of astrophysical implications. Although it is commonly assumed that the IMF is universal and independent of cosmic time, several authors have suggested that the IMF might indeed evolve (Davé 2008; van Dokkum 2008) or depend on the stellar mass of the system (e.g. Worthey, Faber & Gonzalez 1992; Trager et al. 2000a,b; Graves, Faber & Schiavon 2009; Auger et al. 2010b; Graves & Faber 2010; Napolitano, Romanowsky & Tortora 2010; Treu et al. 2010). Recently, van Dokkum & Conroy (2010) have suggested that low-mass stars ($\lesssim 0.3\,{\rm M}_{\odot}$) could be far more dominant in massive ETGs than previously thought. This could imply that much of the increase in the M/L of galaxies with galaxy mass is due to a changing stellar IMF rather than an increasing DM fraction, consistent with the suggestions of Treu et al. (2010) and Auger et al. (2010b).

Valuable additional information on distant ETGs, besides their kinematics, can be provided by gravitational lensing. Strong gravitational lensing provides a very useful tool to investigate the total mass content of the lens (Maoz & Rix 1993; Kochanek et al. 2000; Rusin & Ma 2001; Rusin & Kochanek 2005; Dye & Warren 2005; Brewer & Lewis 2006b, 2008) and to place constraints on the inner mass distribution of lens galaxies at redshift out to $z \simeq 1$. Unfortunately, the mass-sheet and the related mass-profile (Wucknitz 2002) degeneracies do not always allow one to accurately determine the slope of the galaxy density profile and above all to unambiguously disentangle the luminous and DM components.

Gravitational lensing and stellar dynamics are particularly effective to break many of these degeneracies, when they are applied in combination in the analysis of the internal structure of distant ETGs. The two approaches are complementary and allow, when combined self-consistently, to robustly determine the mass profile of the lens galaxy (Koopmans & Treu 2002, 2003; Treu & Koopmans 2002, 2003, 2004; Barnabé & Koopmans 2007; Jiang & Kochanek 2007; Czoske et al. 2008; Barnabé et al. 2009, 2011; Grillo et al. 2009; Koopmans et al. 2009; Treu 2010). Disentangling stellar and DM remains difficult, but the uncertainties have been reduced from factors of a few to far less than this (Treu et al. 2010).

The X-Shooter Lens Survey (XLENS) aims to take the next step, and spectroscopically observe a sample of lens galaxies from the Sloan Lens ACS Survey (SLACS; Bolton et al. 2006) with $\sigma_{\rm ETG} \geq 250\,{\rm km\,s^{-1}}$ using the X-Shooter instrument.[1] With these data we intend to further disentangle the stellar and DM content of the galaxies, through combined lensing, dynamical and *spectroscopic* stellar population studies. With multiband *Hubble Space Telescope* images in hand, we are able to obtain more precise DM mass fractions than ever before, in order to ultimately correlate these with ETG mass, and compare with theoretical galaxy formation models. By combining the lensing and dynamical results with stellar population models, we will plan to constrain the normalization and shape of the stellar IMF.

In this paper, we present the result of a pilot program of the XLENS project: a study of the 'Comic Horseshoe' (SDSS J1148+1930), an almost complete Einstein ring with a diameter of $\sim$10.2 arcsec around a very massive ETG at $z = 0.444$. The system was discovered by Belokurov et al. (2007) in the Sloan Digital Sky Survey Data Release 5 (SDSS DR5; Adelman-McCarthy et al. 2007). The source is a star-forming galaxy at $z = 2.381$ (Dye et al. 2008; Quider et al. 2009). Properties and characteristics of the Cosmic Horseshoe are listed in Table 1, and a composite SDSS image of the system is shown in Fig. 1.

The paper is organized as follows. In Section 2, we present the observations and data reduction. In Section 3, we discuss our kinematic analysis. In Section 4, we discuss the luminous and DM distributions of the lens galaxy. We summarize our findings and present our conclusions in Section 5. We assume $H_0 = 70\,{\rm km\,s^{-1}\,Mpc^{-1}}$, $\Omega_{\rm m} = 0.3$ and $\Omega_{\Lambda} = 0.7$ throughout the paper.

2 OBSERVATIONS AND DATA REDUCTION

X-Shooter observations of SDSS J1148+1930 were carried out during a Guaranteed Time Observation (GTO) run between 2010 March 17 and 24 in slit mode,[2] splitting the beam over three arms:

[1] X-Shooter is a powerful broad-band (3000–25000 Å), three-armed medium-resolution spectrograph on the Very Large Telescope (VLT; D'Odorico et al. 2006); 22 h GTO time on three systems (084.A-0289 and 087.A-0620) and 40 h GTO time were awarded (P086.A-0312) to the XLENS project (PI: Koopmans)

[2] P084.A-0289(A); PI: Koopmans.

Table 1. Properties of the Cosmic Horseshoe[a].

	Parameter	Values
Lens	RA	$11^{h}\,48^{m}\,33\overset{s}{.}15$
Galaxy	Dec.	$19^{\circ}\,30'\,03\overset{''}{.}5$
	Redshift	0.444
	Effective radii	1.96 ± 0.02 arcsec
	g_L	(20.84 ± 0.06) mag
	r_L	(19.00 ± 0.02) mag
	i_L	(18.22 ± 0.01) mag
	z_L	(17.75 ± 0.04) mag
	Axis ratio, g	0.8 ± 0.1
Source	Redshift[b]	$2.381\,15 \pm 0.000\,12$
	Star formation rate	$\sim 100\,M_{\odot}\,yr^{-1}$
	Dynamical mass	$M_{vir} \simeq 10^{10}\,M_{\odot}$
Ring	Diameter	10.2 arcsec
	Length	$\sim 300^{\circ}$
	u_L	21.6 mag
	g_L	20.1 mag
	i_L	19.7 mag
	Mass enclosed[c]	$(5.02 \pm 0.09) \times 10^{12}\,M_{\odot}$

[a]Belokurov et al. (2007) measured the redshift of the source to be $z = 2.379$. We find a systematic shift that brings the source redshift to be $z = 2.3811$ in agreement with Quider et al. (2009).
[b]The mass within the Einstein radius or, more precisely, within the ring diameter is taken from Dye et al. (2008).
[c]Parameters obtained from images taken with the 2.5-m Isaac Newton Telescope. Magnitudes are taken from SDSS DR7. See Belokurov et al. (2007).

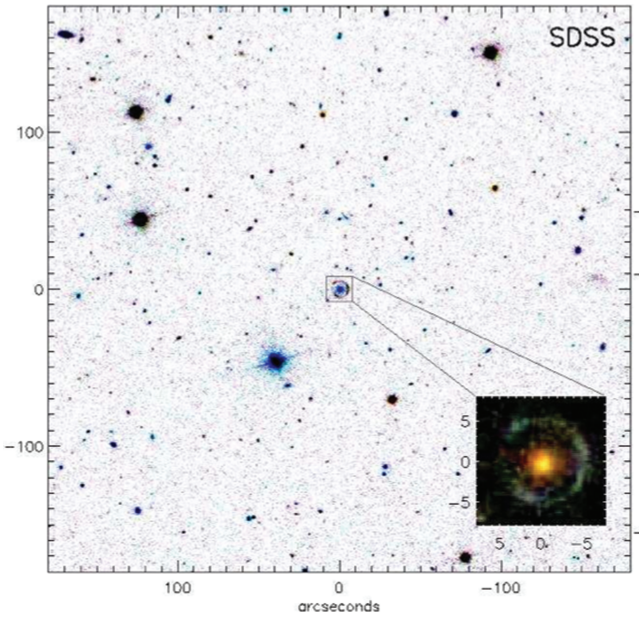

Figure 1. SDSS colour composite image of the sky region around the Cosmic Horseshoe (the zoom is 16×16 arcsec^2).

UVB ($R = 3300$ with 1.6-arcsec slit); VIS ($R = 5400$, with 1.5-arcsec slit) and near-infrared (NIR) ($R = 3300$ with 1.5-arcsec slit), covering a wavelength range from 3000 to 25 000 Å simultaneously. The 11-arcsec long slit was centred on the galaxy with a position angle of 163°. The latter minimizes contamination from the source and leaves enough sky region to facilitate accurate sky subtraction. Two observation blocks (OBs) were not used because of bad seeing and/or an incorrect positioning of the slit on the object. The total exposure time on target for each arm is ∼7389 s and the typical seeing is ∼0.6 arcsec. Standard calibration frames were obtained during daytime after the corresponding OB. A summary of the observing blocks is given in Table 2.

Table 2. Observational details of the Cosmic Horseshoe.

Observation block	Date	Exp. time (s)	Seeing (arcsec)
200200337	2010-17-3	3×821 (*UVB*−VIS) $3 \times 3 \times 274$ (NIR)	0.62
200200343	2010-17-3	3×821 (*UVB*−VIS) $3 \times 3 \times 274$ (NIR)	0.56
200200436	2010-19-3	3×821 (*UVB*−VIS) $3 \times 3 \times 274$ (NIR)	0.66

Data reduction was done using the European Southern Observatory (ESO) X-Shooter pipeline v1.2.1 (Goldoni et al. 2006) and the Gasgano data file organizer developed by ESO. The pipeline reduction uses calibration spectra, taken during the commissioning run, for bias subtraction and flat-fielding of the raw spectra. Cosmic rays are removed using LACosmic (van Dokkum 2001). For each arm, the orders are extracted and rectified in wavelength space using a wavelength solution previously obtained from the calibration frames. The resulting rectified orders are shifted and co-added to obtain the final 2D spectrum. We extract a 1D spectrum from the resulting 2D merged spectrum, using an IDL code that uses the optimal-extraction algorithm of Horne (1986). It also produces the corresponding error file and bad pixel map. The final signal-to-noise (S/N) ratio in the *UVB*+VIS spectrum is ∼7 pixel^{-1}. No telluric correction was applied, so that prominent atmospheric absorption bands can still be seen in the final spectrum (Fig. 2).

Because the NIR spectrum suffers seriously from sky-line residuals using the current pipeline, we limit our analysis to the *UVB*−VIS region of the spectrum and defer a full analysis of the IR data as well as our spectroscopic stellar-population analysis to future work. In this paper, we base our stellar mass determinations solely on the broad-band colours from the SDSS plus the stellar kinematic and lensing data.

3 STELLAR KINEMATICS

We measure the luminosity-weighted velocity dispersion (LOSVD) of the lens galaxy from the final 1D *UVB*−VIS spectrum using the Penalized Pixel Fitting (PPxF) code of Cappellari & Emsellem (2004). PPxF determines the combination of stellar templates which, when convolved with an appropriate LOSVD, best reproduces the galaxy spectrum. The best-fitting parameters of the LOSVD are determined by minimizing a χ^2 penalty function. The best fit provides the mean velocity and the velocity dispersion (v and σ, respectively), plus their uncertainties. The S/N ratio of the data is inadequate to measure the higher order Gauss–Hermite moments h_3 and h_4, which quantify the asymmetric and symmetric departures of the LOSVD from a pure Gaussian (related to the skewness and kurtosis, respectively). PPxF also allows the user to mask noisy or bad regions of the galaxy spectrum. We also perform an iterative sigma-clipping in order to clean the spectrum of residual bad pixels, sky lines and cosmic rays. We focus on absorption lines between 3500 and 5500 Å (including Ca H&K, G4300, H_β, Mg_b and some Fe lines). To minimize errors due to mismatch between the resolution

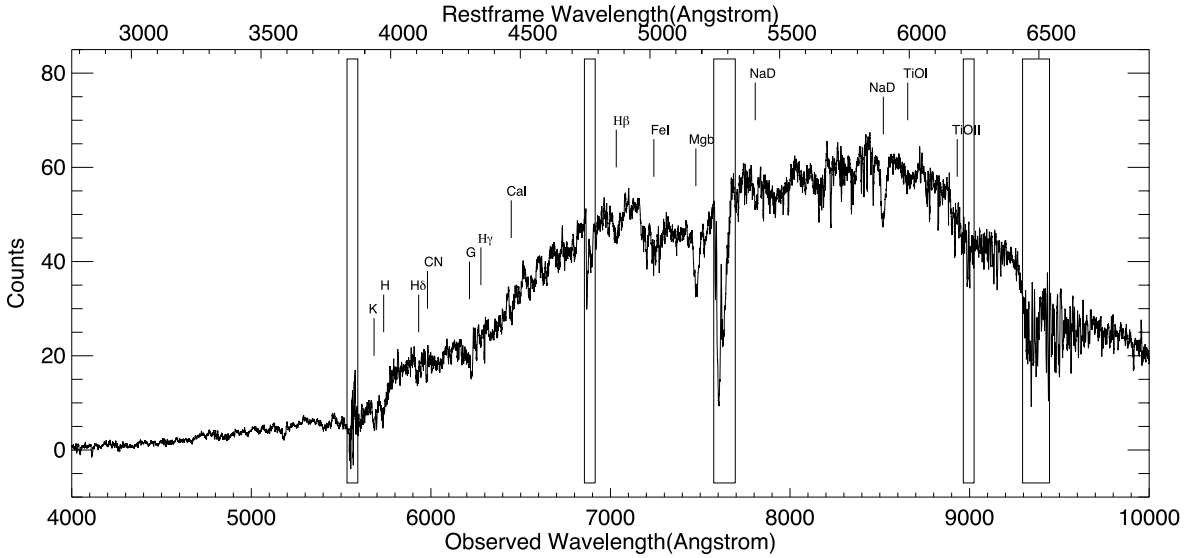

Figure 2. The final luminosity-weighted *UVB*−VIS 1D X-Shooter spectrum extracted from a rectangular aperture of $1.8 \times 1.6\,\mathrm{arcsec}^2$ centred on the galaxy (see text). Spectral features the lens galaxy are marked. Telluric absorption lines have not been removed from the spectrum nor has the spectrum been flux-calibrated. The boxes indicate parts of spectrum that are affected by sky or telluric lines.

of the templates and the galaxy spectrum, we use X-Shooter stellar spectra obtained as part of the X-Shooter Stellar Library (XSL) survey (Trager et al., in preparation), with similar instrumental resolution (for the galaxy spectrum we use a 1.5-arcsec slit, corresponding to $\sigma_{\mathrm{instr}} \sim 25\,\mathrm{km\,s^{-1}}$, while for the stellar templates the slit width is 0.7 arcsec, corresponding to $\sigma_{\mathrm{instr}} \sim 12\,\mathrm{km\,s^{-1}}$). An excellent fit is obtained with a weighted linear combination of a K1 giant template (57 per cent) and a G2 star template (43 per cent). The selected region of our galaxy spectrum used for the fit and the corresponding best-fitting stellar template are shown in Fig. 3.

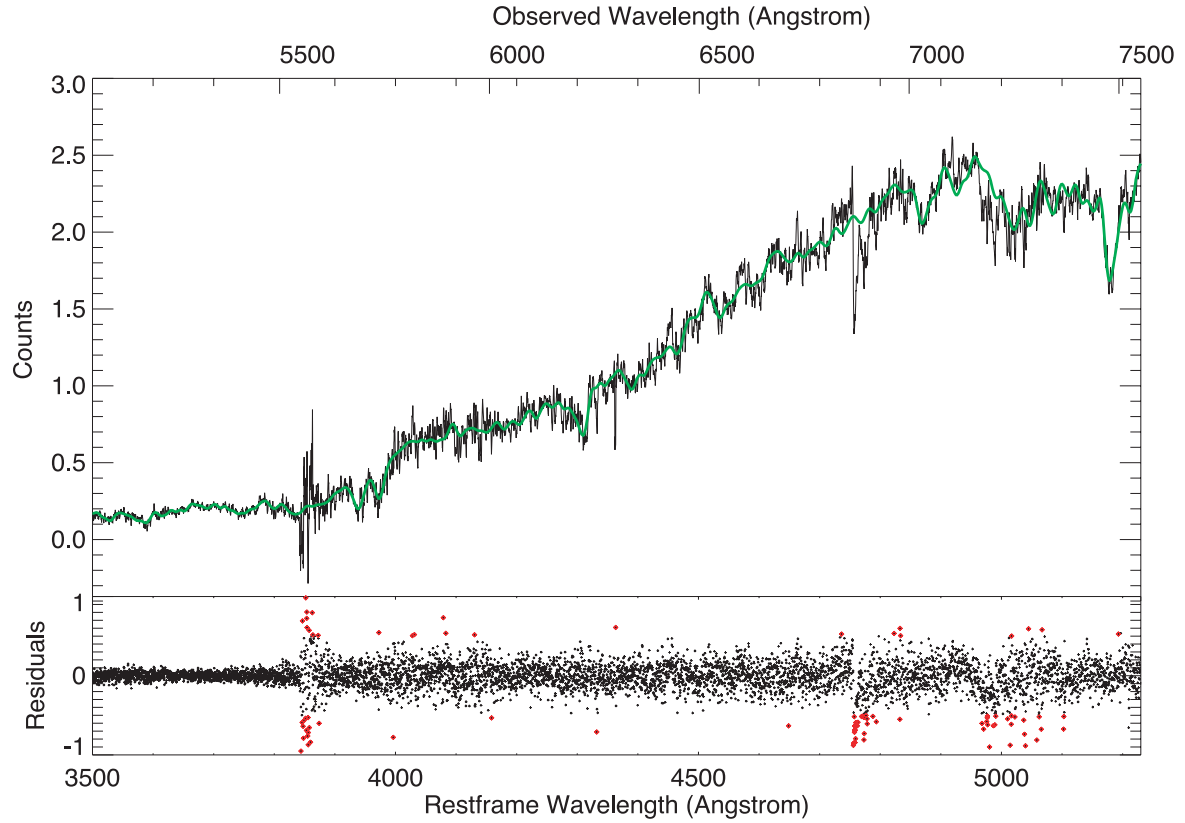

Figure 3. Top panel: logarithmically rebinned *UVB*+VIS galaxy spectrum (black) and logarithmically rebinned best-fitting template (green), both in rest-frame wavelength. Bottom panel: residuals from the fit. Bad pixels excluded from the fitting procedure (sky line, telluric lines) are shown in red. See text for more information.

3.1 Luminosity-weighted kinematics

The measured luminosity-weighted velocity distribution[3] for the central aperture of 1.8×1.6 arcsec^2 is $\langle\sigma\rangle = 352 \pm 10 \pm 16\,\mathrm{km\,s^{-1}}$. The formal error on the dispersion includes both the random error contribution and the systematic uncertainties due to spectral range differences, template mismatch and continuum fitting as discussed below. Fig. 3 shows the best-fitting template of the PPxF routine superimposed on the galaxy spectrum as well as the residuals of the fit.

As a first test of the accuracy of our measurements, we use the more heterogeneous MILES[4] stellar template library (Sánchez-Blázquez et al. 2006). We select 100 stars (F, G, K, M) in the range 3525–7500 Å, with 2.3 Å full width at half-maximum (FWHM) spectral resolution. The measured luminosity-weighted stellar velocity dispersion of $\langle\sigma\rangle = 358 \pm 31\,\mathrm{km\,s^{-1}}$, after instrumental correction, is consistent with the above estimate, based on XSL templates, but has larger errors due to the lower resolution of the MILES library. As a second test, we fit templates to two different spectral regions. We find slightly different results between the blue and the red part of the spectrum, but always consistent within 2σ (not including systematics). The scatter in these fits is used to estimate additional systematic uncertainties related to template mismatches and spectra coverage.

3.2 Spatially resolved kinematics

To preserve the spatially resolved kinematic information, we define seven spatially varying apertures (with adequate S/N ratio) along the radial direction, and we sum the signal within each aperture. Apertures are defined to be larger than the seeing, in order to have independent kinematics measurements for each aperture. The stellar rotation velocity and velocity dispersion are measured in each aperture using PPxF, as described above. Again, we use different spectral regions, excluding the most prominent telluric lines in the VIS range and a range of seven XSL stellar templates (G, K and M stars). The uncertainties on the inferred kinematics are estimated by adding in quadrature the formal uncertainty given by PPxF and the scatter in the results for different templates and spectral regions. Details of the aperture sizes and the kinematic profiles are listed in Table 3. The rotation and the velocity dispersion profiles are shown in Fig. 4.

We find an almost flat velocity dispersion profile beyond the effective radius. The weighted average value of $344 \pm 25\,\mathrm{km\,s^{-1}}$ is consistent within the formal error with the luminosity-weighted value for an aperture of 1.8×1.6 arcsec^2 (see Table 3), as expected. The velocity profile shows some mild rotation, with a projected rotation velocity of $\sim$140 km s^{-1} at one effective radius. Because the effective dispersion ($v_{\mathrm{rms}}^2 = \sqrt{v^2 + \sigma^2}$; see Cappellari 2008) is well within the errors on σ, the effect of rotation can be neglected in our spherical Jeans analysis and we will ignore rotation in the remainder of this paper.

[3] The only velocity dispersion value previously published for the Cosmic Horseshoe is from Belokurov et al. (2007). They perform fits of Gaussian line profiles to the Ca H&K absorption lines from a much lower resolution spectrum (FWHM $\sim$ 10 Å). They find a higher velocity dispersion estimation of $430 \pm 50\,\mathrm{km\,s^{-1}}$, in consistent with our high-quality data.

[4] http://www.iac.es/proyecto/miles/pages/stellar-libraries/miles-library.php

Table 3. Spatially resolved kinematics of the Cosmic Horseshoe.

Aperture centre (arcsec)	Aperture dimension (arcsec)	v (km s^{-1})	σ (km s^{-1})
0.00, 0.00	1.80×1.60	0 ± 15	352 ± 10
−2.16, 0.00	0.80×1.60	-100 ± 100	350 ± 100
−1.36, 0.00	0.80×1.60	-80 ± 100	311 ± 76
−0.64, 0.00	0.64×1.60	-9 ± 25	341 ± 26
0.00, 0.00	0.64×1.60	0 ± 12	332 ± 16
+0.64, 0.00	0.64×1.60	62 ± 18	360 ± 25
+1.36, 0.00	0.80×1.60	77 ± 80	350 ± 100
+2.16, 0.00	0.80×1.60	180 ± 100	410 ± 100

4 STELLAR AND DARK MATTER

Here we derive the slope of the total density profile and calculate the fraction of DM inside one effective radius.

4.1 The galaxy mass model

To derive the stellar mass inside the Einstein radius, we follow Treu & Koopmans (2002), Koopmans & Treu (2003) and Treu & Koopmans (2004). We model the mass distribution as a superposition of the stellar and the DM components. For the stellar mass distribution, we use two different spherical models, described by the equation:

$$\rho_*(r) = \frac{(3-n)M_* r_*}{4\pi r^n (r + r_*)^{4-n}}. \quad (1)$$

The Hernquist (1990) luminosity–density profile has $n = 1$, and the Jaffe (1983) luminosity–density profile has $n = 2$. The total stellar mass is M_* and the break radius is r_*.

We model the DM distribution as a generalized spherical Navarro–Frenk–White profile, using a break radius of $r_{\mathrm{b}} = 50$ kpc, which is typical of massive ETGs (although the result is insensitive to its exact value) and an outer slope of $\gamma_{\mathrm{out}} = 3$ (Gavazzi et al. 2007; Auger et al. 2010a), following the prediction from numerical simulations of DM haloes (Ghigna et al. 2000):

$$\rho_{\mathrm{DM}}(r) = \frac{\rho_{\mathrm{d},0}}{(r/r_{\mathrm{b}})^{-\gamma}\left[1 + (r/r_{\mathrm{b}})^2\right]^{(\gamma-3)/2}}. \quad (2)$$

The break radius and the density scale ($\rho_{\mathrm{d},0}$) determine the virial mass of the DM halo (Bullock et al. 2001).

For completeness, we also use a single mass component model where the stellar and DM mass densities add to a power law with an effective density slope γ' for $\rho_{\mathrm{tot}} \propto r^{-\gamma'}$, and the stars are treated as trace particles (see Koopmans & Treu 2003).

The most accurately known constraint from the lens mass model is the mass inside the Einstein radius. We use $M_{\mathrm{E}} = (5.02 \pm 0.09) \times 10^{12}\,\mathrm{M}_\odot$ inside $\theta_{\mathrm{E}} = 5.1$ arcsec derived by Dye et al. (2008). The mass components must add to M_{E} within the Einstein radius. The error in radius is folded into the error in mass so that a fixed radius can be used (the mass and Einstein radius are coupled in the modelling). We use the average of the two effective radii from the *g*- and *i*-band images reported in Belokurov et al. (2007), $R_{\mathrm{eff}} = 1.96 \pm 0.02$ arcsec (Table 1). The effective radius is uniquely related to r_* (see Hernquist 1990; Jaffe 1983).

We also assume a constant orbital anisotropy parameter β and allow it to range between 0.0 and 0.5, which is typical for massive ETGs (e.g. Gerhard et al. 2001). The parameters of the model without a strong prior are then the stellar mass (M_*) and the DM density slope (γ), or only γ' for the single-component model.

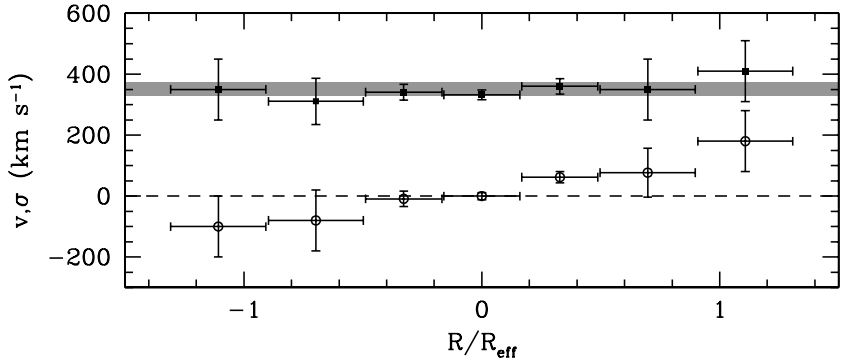

Figure 4. Kinematic profiles of the Cosmic Horseshoe. Rotation (bottom) and velocity dispersion (top). Grey line shows the light-weighted value for the central aperture.

We subsequently solve the spherical Jean equations and compare the models to the kinematic data, taking the aperture sizes and seeing into account. We find an effective density slope of

$$\gamma' = 1.72^{+0.05}_{-0.06} \quad [68 \text{ per cent confidence level (CL)}],$$

when marginalizing over $\beta = 0.0$–0.5, shallower than isothermal (see Koopmans et al. 2006, 2009). This slightly low value for the logarithmic total-density slope may suggest that this object can be a group, or a small cluster of galaxies, where the overall efficiency of converting gas into stars is lower, and where typically the overall mass density profile in the corresponding region is shallower than isothermal (e.g. Newman et al. 2011). Changing the luminosity–density profile also does not change the final logarithmic slope significantly. The more interesting case of the two-component model will now be discussed.

4.2 The stellar mass fraction from lensing and kinematic constraints

To derive the stellar mass fraction inside the Einstein radius, we create a densely sampled grid of likelihood values by comparing the kinematic profiles to the data for a projected stellar mass fraction [$f^*(<R_E)$] within the Einstein radius ranging between 0 and 1 and a DM density slope (γ) ranging between 0.0 and 2.0. We assume flat priors on both quantities and marginalize over γ to derive the probability density function (PDF) of $f^*(<R_E)$. The results for the Hernquist and Jaffe profiles are shown in Fig. 5 for $\beta = 0$ and a more extreme case of radial anisotropy with $\beta = 0.5$. Taking as reference the best-fitting parameters of the Sérsic profile computed in Dye et al. (2008): $n = 5.40 \pm 0.04$, $r_0 = 3.9 \pm 0.1$, $L_{1/2} = 61.2 \pm 0.4$), with the form

$$L = L_{1/2} \exp\left\{-B(n)\left[(r/r_0)^{1-n} - 1\right]\right\}, \quad (3)$$

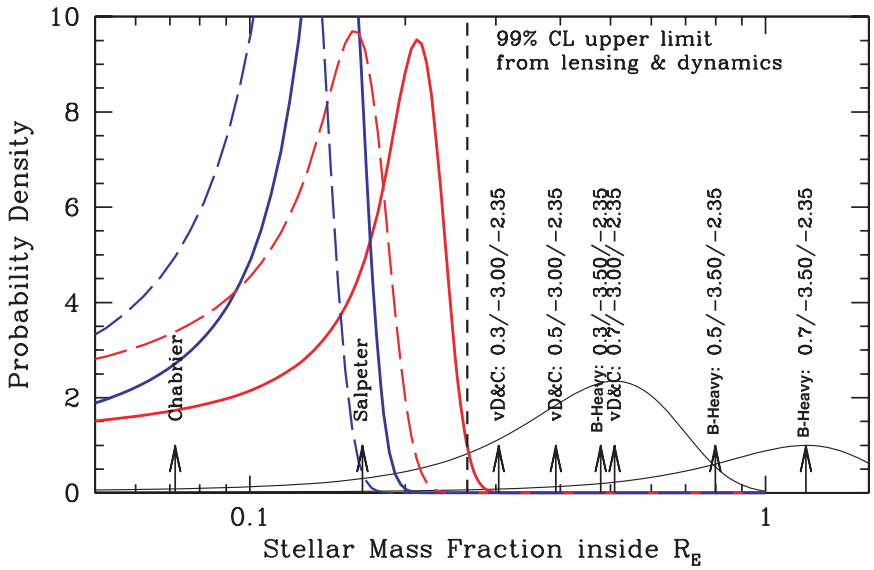

Figure 5. Marginalized PDF for the Hernquist model (red lines) and the Jaffe model (blue lines) from our lensing and dynamics model. Solid lines are for an anisotropy parameter of $\beta = 0.0$, and dashed lines for $\beta = 0.5$. Black arrows show the internal stellar mass fractions with different IMFs from our stellar population analysis. Black lines represent PDFs of van Dokkum & Conroy IMF and of the most extreme bottom-heavy IMFs. In the labels, the first number represents the break radius, the second is the IMF slope at lower masses ($m \leq m_{\rm break}$) and the last number is the slope at higher masses (fix to Salpeter slope). We exclude the Chabrier IMF and the $\alpha = -3$ IMFs at a CL of $\geq$90 per cent and the extreme bottom-heavy ($\alpha = -3.5$) IMFs at a CL of 99 per cent, while the Salpeter IMF is fully consistent with lensing data.

we conclude that Hernquist and Jaffe profiles fit well the observed luminosity profile of the galaxy within the effective radius (with a slight preference for the Hernquist model).

We find a fraction of stellar mass within the Einstein radius for the two luminosity profiles of

$$f^*_{\rm HQ} = 0.19^{+0.04}_{-0.09} \quad \text{and} \quad f^*_{\rm JF} = 0.13^{+0.03}_{-0.05} \quad \text{for } \beta = 0$$

and

$$f^*_{\rm HQ} = 0.13^{+0.04}_{-0.07} \quad \text{and} \quad f^*_{\rm JF} = 0.11^{+0.02}_{-0.05} \quad \text{for } \beta = 0.5.$$

We note that in projection the lens galaxy is already fully DM-dominated inside ∼2.5 effective radii. For comparison with previous work, we also derive the DM fraction inside the effective radius and find

$$f_{\rm DM}(< R_{\rm eff}) = 0.60^{+0.15}_{-0.06} \pm 0.1,$$

(68 per cent CL) for $\beta = 0$, including a systematic uncertainty of 0.1. The random error is based on the marginalized probability densities shown in Fig. 5, and a systematic error is included based on the maximum range of possible DM density slopes. Although the latter is constrained by the models, we extrapolate inwards from $R_{\rm E}$ to $R_{\rm eff}$, where this slope could be somewhat different. We note though that the systematic error is rather conservative. The DM fraction increases by ∼0.1 for $\beta = 0.5$ and the difference between the Hernquist and Jaffe profiles is negligible (by construction, since they both contain equal fractions of mass inside that radius). This high DM fraction inside the effective radius is consistent with the result found in Auger et al. (2010b) for SLACS systems and is consistent with the DM fraction within the effective radii being a monotonically increasing function of galaxy mass.

4.3 Stellar mass fraction from stellar population constraints

We independently calculate the projected stellar mass fraction inside the Einstein radius using stellar population synthesis models and the SDSS colours (see Table 1) of the lens galaxy. A comparison between this fraction and that derived from lensing and stellar kinematics provides a direct constraint on the stellar IMF (see also e.g. Auger et al. 2010b; Treu et al. 2010).

We use GALAXEV, a library of evolutionary stellar population synthesis models computed using the isochrone synthesis code of Bruzual & Charlot (2003). This code allows one to compute the spectral evolution of stellar populations for a wide range of ages and metallicities. Here we use the 2007 version of GALEXEV kindly provided by S. Charlot (a version commonly known as 'CB07'). We use six simple stellar populations (SSP) models computed with a Salpeter IMF or a Chabrier IMF for a range of metallicities from $Z = 0.0001$ to 0.05, all of them with lower mass cut-off of $M_{\rm low} = 0.1\,{\rm M}_\odot$ and upper mass cut-off of $M_{\rm up} = 100\,{\rm M}_\odot$. The spectral resolution is 3 Å across the wavelength range of 3200–9500 Å.

We compute the spectral evolution of the stellar population and the redshift dependence of colours and magnitudes in the SDSS filters g, r, i and z for all SSP models and for a range of ages and star formation histories (SFHs). For the SFH model, we use an exponentially declining star formation rate (SFR) with time-scales $\tau = 0.1$–0.4 Gyr and as extreme cases an instantaneous burst with $\tau = 0$ or a constant SFR. We compute the redshift evolution of the galaxy colours and magnitudes for a start of star formation between 12 and 5 Gyr, corresponding to a formation redshift of between roughly $z \sim 5$ and ∼0.5. By comparing the model magnitudes to the SDSS magnitudes, we subsequently determine a grid (as function of age, metallicity and SFH duration) of likelihood values for each model as well as the total stellar mass. We do this for both the Salpeter and Chabrier IMFs.

We use the standard Bayesian approach, as outlined in Auger et al. (2009), to determine the posterior PDF and the marginalized errors on the total stellar mass of the galaxy, assuming flat priors on all parameters in logarithmic space (e.g. a prior $\propto 1/\tau$ for τ). The latter assumption is not critical, but given that the time-scales of the SFH, etc., are unknown a priori, this prior is a better description of our ignorance before making the observations (and modelling). From the resulting cumulative probability function, we calculate the median of the total stellar mass and its 68 per cent confidence interval for both IMFs. Using the observed brightness profile of the galaxy modelled as a Hernquist, Jaffe or deVaucoulers profiles (the precise choice is not critical), we determine the fraction of the stellar mass (assuming a constant M/L ratio) within the Einstein radius. The results of this analysis are listed in Table 4, where we report the inferred total stellar mass fraction for each IMF as well as that from lensing and kinematics.

We find that, for the range of assumed luminous profiles and anisotropies, the stellar mass fraction from lensing agrees remarkably well with that from stellar population modelling assuming a Salpeter IMF (Fig. 5). This result further supports the results found by Treu et al. (2010) that the IMF of massive early-type lens galaxies is well matched by an evolved Salpeter IMF. They found a tentative trend of the IMF slope with galaxy velocity dispersion, with a 'light' IMF such as a Chabrier IMF is inappropriate for systems with $\sigma \geq 200\,{\rm km\,s^{-1}}$. This trend may imply a non-universal IMF, perhaps dependent on metallicity, age or abundance ratios of the stellar populations. Alternatively, it may imply non-universal DM haloes with inner density slope increasing with velocity dispersion. While the degeneracy between the two interpretations cannot be broken without additional information, Treu et al. data imply that massive ETGs cannot have both a universal IMF and universal DM haloes. This is confirmed by the expanded analysis of Auger et al. (2010b), who added weak-lensing data to constrain the halo model, finding that the data for massive galaxies are inconsistent with a Chabrier universal IMF for a range of realistic halo profiles, including various recipes to account for baryonic effects.

5 BOTTOM-HEAVY IMFS

Recently, van Dokkum & Conroy (2010) have suggested the presence of a large number of stars with masses $\leq 0.3\,{\rm M}_\odot$ in the central regions of ETGs. By measuring the strength of the NaI doublet and the Wing–Ford molecular FeH band in the spectra of eight of the most luminous and massive ETGs in the Virgo and Coma clusters, they infer that the IMF for these systems might even be steeper than Salpeter, with a slope as steep as $\alpha = -3$. They also test even more 'bottom-heavy', with $\alpha = -3.5$, and 'bottom-light' (dwarf deficient) IMFs, but they find the best fit between stellar population synthesis models and spectrum around the NaI doublet with the $\alpha = -3$ IMFs, although the uncertainties are large and Salpeter cannot be excluded with high confidence.

Here, we investigate this claim by assuming a broken power-law IMF, with the Salpeter slope in the high-mass regime that dominates the SDSS magnitudes (i.e. changes in the IMF below this break do not affect the stellar-population analysis carried out above) and a steeper profile in the low-mass range. We test three different values of the break point in the mass function: $m_{\rm break} = 0.3$, 0.5 and $0.7\,{\rm M}_\odot$, respectively. Changing the IMF for stars with $M \leq m_{\rm break}$ does not change the SDSS colours because $\gtrsim$90 per cent of the light in the spectral region we studied here is coming from stars with

Table 4. The stellar mass fractions within the Einstein Radius derived from lensing plus stellar kinematics and from stellar population synthesis models, respectively. The likelihood ratio compares maximum a posteriori difference between the SSP model and the no-difference (null-hypothesis) model with the isotropic Hernquist model, which has the highest inferred stellar mass fraction. The IMF slope is assumed to be $\alpha = -2.35$ beyond the break $m_{\rm break}$ in the mass function. The probabilities in between parentheses represent for each IMF the fraction probability that a given PDF (P_0) matches the max probability.

Lensing and kinematic model	Anisotropy	Stellar mass fraction	
Hernquist	$\beta = 0.0$	$0.19^{+0.04}_{-0.09}$	
	$\beta = 0.5$	$0.13^{+0.04}_{-0.07}$	
Jaffe	$\beta = 0.0$	$0.13^{+0.03}_{-0.05}$	
	$\beta = 0.5$	$0.11^{+0.02}_{-0.05}$	
Stellar population model	$m_{\rm break}$ ($\mathrm{M}_\odot$)	Stellar mass fraction	$2\ln(P_{\rm max}/P_0)$ (HQ versus SSP)
Chabrier	–	0.07 ± 0.02	3.0 (0.08)
Salpeter	–	0.17 ± 0.06	0.1 (0.75)
van Dokkum & Conroy $\alpha = -3.0$	0.3	0.30 ± 0.11	1.0 (0.32)
van Dokkum & Conroy $\alpha = -3.0$	0.5	0.39 ± 0.15	1.9 (0.17)
van Dokkum & Conroy $\alpha = -3.0$	0.7	0.51 ± 0.18	3.0 (0.08)
Bottom-heavy $\alpha = -3.5$	0.3	0.48 ± 0.17	2.8 (0.09)
Bottom-heavy $\alpha = -3.5$	0.5	0.80 ± 0.29	4.5 (0.03)
Bottom-heavy $\alpha = -3.5$	0.7	1.19 ± 0.43	5.0 (0.03)

$M \geq 0.7\,\mathrm{M}_\odot$. On the other hand, it dramatically changes the total stellar mass of the system, because stars with masses of 0.1–0.3 $\mathrm{M}_\odot$ can contribute at least 60 per cent of the stellar mass for these bottom-heavy IMFs.

We calculate the change in total stellar mass arising from the change in the slope of the IMF:

$$\Delta M = \int_{0.1\,\mathrm{M}_\odot}^{m_{\rm break}} \left[\left.\frac{\mathrm{d}N}{\mathrm{d}m}\right|_{\rm IMF} - \left.\frac{\mathrm{d}N}{\mathrm{d}m}\right|_{\rm Salp} \right] m\,\mathrm{d}m, \quad (4)$$

where

$$\left.\frac{\mathrm{d}N}{\mathrm{d}m}\right|_{\rm IMF} = \begin{cases} \left(\dfrac{m}{m_{\rm break}}\right)^{\eta} & \text{if } m_{\rm break} < m \leq 100\,\mathrm{M}_\odot \\ \left(\dfrac{m}{m_{\rm break}}\right)^{\alpha} & \text{if } 0.1\,\mathrm{M}_\odot < m \leq m_{\rm break} \end{cases}, \quad (5)$$

with $\eta = -2.35$ (Salpeter slope), $\alpha = -3$ for the bottom-heavy IMFs suggested by van Dokkum & Conroy (2010) or $\alpha = -3.5$ in the most extreme case.

Our results for the bottom-heavy stellar mass fraction are listed in Table 4. We also list the likelihood ratios between the nominal isotropic Hernquist model lensing and dynamic stellar mass fraction and the stellar mass fractions obtained from stellar populations and colours for the different IMFs (equivalent to $\Delta\chi^2$ if the distribution was Gaussian, which we assume as a first approximation), comparing their maximum a poteriori difference with the no-difference hypothesis. Vertical arrows in Fig. 5 show the stellar mass fractions predicted by stellar population synthesis models and SDSS colour by these different IMFs and the stellar mass fraction obtained with lensing and dynamics. Using $m_{\rm break} = 0.7\,\mathrm{M}_\odot$ and a bottom-heavy IMF, we find that inferred stellar mass fraction exceeds unity for $\alpha = -3.5$, inconsistent with the lensing mass. An extreme 'bottom-heavy' IMF with slope of $\alpha = -3.5$ is inconsistent at the >90 per cent CL with the lensing and kinematic results. The $\alpha = -3$ model is only marginally consistent for $m_{\rm break} = 0.3$, but is also excluded at the >90 per cent CL for $m_{\rm break} = 0.7$. A Salpeter IMF gives the best agreement with the lensing and kinematics. It is important to mention that we do not include any possible effects of large-scale structure LOS contamination (e.g. from a group elongated along the LOS) that would decrease the total mass assumed here. Recalling Treu et al. (2009) and Guimarães & Sodré (2011), SLACS lenses are shown to be unbiased sample in relation to a random LOS, despite the fact that the lenses are elliptical galaxies which are often found in dense regions. Moreover, other possible explanations, such as a top-heavy IMF with more black holes and neutron stars remnants, are still possible. As discussed in van Dokkum (2008), top-heavy IMFs have fewer low-mass stars than a standard Salpeter IMF but many more high-mass stars. Nevertheless, it is important to clarify that since our method only infers the overall *M*/*L* ratio, we cannot distinguish a Salpeter IMF from a bottom-light IMF like a Chabrier IMF due to the presence of remnants (Treu et al. 2010; Auger et al. 2010b).

6 SUMMARY AND CONCLUSIONS

In this paper we present the first results from a new spectroscopic survey of massive early-type lens galaxies: the XLENS. The combination high-fidelity UVIS -IR spectroscopy from the X-Shooter instrument on the VLT, with the strong gravitational lensing mass determination has enabled us to conduct an in-depth study of the internal structure of the luminous elliptical galaxy SDSS J1148+1930 at $z = 0.444$. We find the following.

(i) The luminosity-weighted stellar velocity dispersion is $\langle\sigma_*\rangle(\lesssim R_{\rm eff}) = 352 \pm 10 \pm 16\,\mathrm{km\,s^{-1}}$, more accurate and considerably lower than a previously published value of $\sim$450 $\mathrm{km\,s^{-1}}$.

(ii) A single-component (stellar plus dark) mass model of the lens galaxy yields a logarithmic total-density slope of $\gamma' = 1.72^{+0.05}_{-0.06}$ (68 per cent CL; $\rho_{\rm tot} \propto r^{-\gamma'}$).

(iii) The projected stellar mass fraction, derived solely from the lensing and dynamical data, is $f_*(<R_{\rm E}) = 0.19^{+0.04}_{-0.09}$ (68 per cent CL) inside the Einstein radius for a Hernquist profile and no anisotropy. The DM fraction inside the effective radius

$f_{\rm DM}(<R_{\rm eff}) = 0.60^{+0.15}_{-0.06} \pm 0.1$ (68 per cent CL), where the latter error is systematic.

(iv) Based on the SDSS colours, we find $f_{*,\rm Salp}(<\rm R_E) = 0.17 \pm 0.06$ for a Salpeter IMF and $f_{*,\rm Chab}(<\rm R_E) = 0.07 \pm 0.018$ for a Chabrier IMF. A Salpeter IMF gives the best agreement between lensing and dynamics constraints on the stellar mass fraction, therefore it is preferred to a Chabrier IMF. Dwarf-rich IMFs with $\alpha \geq 3$ (with $\rm d\mathit{N}/d\mathit{M} \propto \mathit{M}^{-\alpha}$) in the lower mass range of 0.1–0.7 $\rm M_\odot$ – such as those recently suggested by van Dokkum & Conroy (2010) for massive ETGs ($\alpha = -3$) – are excluded at the >90 per cent CL and in some cases ($\alpha = -3.5$) violate the total lensing-derived mass limit.

This massive ETG lies at the extreme end of the trend found by e.g. Auger et al. (2010b) that the DM fraction within the effective radii is a monotonically increasing function of galaxy mass. In fact, SDSS J1148+1930 is already DM-dominated within that region. We find that a Salpeter IMF agrees best with the total stellar mass derived from lensing and stellar kinematics as well as with its SDSS colours. As in Treu et al. (2010) and Grillo & Gobat (2010), a Salpeter IMF appears to be the best option for very massive ETGs, although slightly more massive IMFs cannot be excluded given the typical uncertainties. A bottom-light IMF such as a Chabrier (or Kroupa) IMF agrees only marginally and we exclude a steep 'dwarf-rich' IMF with $\alpha = -3.5$ at >90 per cent CL. Somewhat shallower IMFs with $\alpha \approx -3.0$, as suggested by van Dokkum & Conroy (2010), are marginally acceptable. We conclude that our data are *fully* consistent with SDSS J1148+1930 being a massive ETG that is DM-dominated inside its effective radius and having a Salpeter IMF. No strong evidence for an even more bottom-heavy IMF is found, consistent with previous results (Treu et al. 2010), although uncertainties are still large. Further studies are required to break the degeneracy between the central DM fraction and distribution and the stellar IMF. In forthcoming papers of the XLENS survey, we will extend the study to more massive systems at $z \gtrsim 0.5$ and also a subsample of SLACS lenses at $z \lesssim 0.5$. Observations are ongoing. In those papers, we will perform more detailed stellar population analyses using the full UV–optical–NIR spectrum and obtain independent constraints on the physical parameters that may correlate with IMF normalization (i.e. age and metallicity) or that may be the cause of the correlation between DM content and velocity dispersion.

ACKNOWLEDGMENTS

The authors thank the referee for providing constructive comments and help in improving the contents of this paper.

The use of the PPxF developed by Cappellari & Emsellem and of the GALAXEV software by Bruzual & Charlot are gratefully acknowledged. Data were reduced using EsoRex and XSH pipeline by ESO Data Flow System Group. We thank Professor P. Groot for instruction on its use. CS acknowledges support from an Ubbo Emmius Fellowship. LVEK is supported in part by an NWO-VIDI program subsidy (project number 639.042.505). TT acknowledges support from a Packard Research Fellowship.

REFERENCES

Adelman-McCarthy J. et al., 2007, ApJS, 172, 634
Arnaboldi M. et al., 1996, ApJ, 472, 145
Auger M. W., Treu T., Bolton A. S., Gavazzi R., Koopmans L. V. E., Marshall P. J., Bundy K., Moustakas L. A., 2009, ApJ, 705, 1099
Auger M. W., Treu T., Bolton A. S., Gavazzi R., Koopmans L. V. E., Marshall P. J., Moustakas L. A., Burles S., 2010a, preprint (arXiv:1007.2880A)
Auger M. W., Treu T., Gavazzi R., Bolton A. S., Koopmans L. V. E., Marshall P. J., 2010b, ApJ, 721, L163
Barnabé M., Koopmans L. V. E., 2007, ApJ, 666, 726
Barnabé M., Czoske O., Koopmans L. V. E., Treu T., Bolton A. S., Gavazzi R., 2009, MNRAS, 399, 21
Barnabé M., Czoske O., Koopmans L. V. E., Treu T., Bolton A. S., 2011, MNRAS, 415, 2215
Belokurov V. et al., 2007, ApJ, 671, L9
Bertin G. et al., 1994, A&A, 292, 381
Binney J., Mamon G. A., 1982, MNRAS, 200, 361
Bolton A. S., Burles S., Koopmans L. V. E., Treu T., Moustakas L. A., 2006, ApJ, 638, 703
Borriello A., Salucci P., Danese L., 2003, MNRAS, 341, 1109
Brewer B. J., Lewis G. F., 2006, ApJ, 637, 608
Brewer B. J., Lewis G. F., 2008, MNRAS, 390, 39
Bruzual G., Charlot S., 2003, MNRAS, 344, 1000
Bullock J. S., Kolatt T. S., Sigad Y., Somerville R. S., Kravtson A. V., Klypin A. A., Primack J. R., Dekel A., 2001, MNRAS, 321, 598
Cappellari M., 2008, MNRAS, 390, 71
Cappellari M., Emsellem E., 2004, PASP, 116, 138
Cappellari M. et al., 2006, MNRAS, 366, 1126
Carollo C. M., de Zeeuw P. T., van der Marel R. P., Danziger I. J., Qian E. E., 1995, ApJ, 441, L25
Czoske O., Barnabé M., Koopmans L. V. E., Treu T., Bolton A. S., 2008, MNRAS, 384, 987
Davé R., 2008, MNRAS, 385, 147
Davis M., Efstathiou G., Frenk C. S., White S. D. M., 1985, ApJ, 292, 371
D'Odorico S. et al., 2006, in McLean I. S., Iye M., eds, Proc. SPIE Vol. 6269, Ground-based and Airborne Instrumentation for Astronomy. SPIE, Bellingham, 626933
Dye S., Warren S. J., 2005, ApJ, 623, 31
Dye S., Evans N. W., Belokurov V., Warren S. J., Hewett P., 2008, MNRAS, 388, 384
Fabbiano G., 1989, ARA&A, 27, 87
Franx M., van Gorkom J. H., de Zeeuw P. T., 1994, ApJ, 436, 642
Frenk C. S., 1985, Nat, 317, 595
Gavazzi R., Treu T., Rhodes J. D., Koopmans L. V. E., Bolton A. S., Burles S., Massey R. J., Moustakas L. A., 2007, ApJ, 667, 176
Gerhard O. E., 1993, MNRAS, 265, 213
Gerhard O., Kronawitter A., Saglia R., Bender R., 2001, AJ, 121, 1936
Ghigna S., Moore B., Governato F., Lake G., Quinn T., Stadel J., 2000, ApJ, 544, 616
Goldoni P., Royer F., François P., Horrobin M., Blanc G., Vernet J., Modigliani A., Larsen J., 2006, in McLean I. S., Iye M., eds, Proc. SPIE, Vol. 6269, Ground-based and Airborne Instrumentation for Astronomy. SPIE, Bellingham, p. 62692K
Graves G. J., Faber S. M., 2010, ApJ, 717, 803
Graves G. J., Faber S. M., Schiavon R. P., 2009, ApJ, 693, 486
Grillo C., Gobat R., 2010, MNRAS, 402, L67
Grillo C., Gobat R., Lombardi M., Rosati P., 2009, A&A, 501, 461
Guimarães A. C. C., Sedré L., Jr, 2011, ApJ, 728, 33
Hernquist L., 1990, ApJ, 356, 359
Horne K., 1986, PASP, 98, 609
Jaffe W., 1983, MNRAS, 202, 995
Jiang G., Kochanek C. S., 2007, ApJ, 671, 1568J
Kochanek C. S. et al., 2000, ApJ, 543, 131
Koopmans L. V. E., Treu T., 2002, ApJ, 568, L5
Koopmans L. V. E., Treu T., 2003, ApJ, 583, 606
Koopmans L. V. E., Treu T., Bolton A. S., Burles S., Moustakas L. A., 2006, ApJ, 649, 599
Koopmans L. V. E. et al., 2009, ApJ, 703, L51
Loewenstein M., White R. E., 1999, ApJ, 518, 50
Maoz D., Rix H.-W., 1993, ApJ, 416, 425
Matsushita K., Makishima K., Ikebe Y., Rokutanda E., Yamasaki N., Ohashi T., 1998, ApJ, 499, L13
Mould J. R., Oke J. B., de Zeeuw P. T., Nemec J. M., 1990, AJ, 99, 1823

Napolitano N. R., Romanowsky A. J., Tortora C., 2010, MNRAS, 405, 2351
Newman A. B., Treu T., Ellis R. S., Sand D., 2011, ApJ, 728, L39
Padmanabhan N. et al., 2004, New Astron., 9, 329
Quider A. M., Pettini M., Shapley A. E., Steidel C. C., 2009, MNRAS, 398, 1263
Rix H., de Zeeuw P. T., Cretton N., van der Marel R. P., Carollo C. M., 1997, ApJ, 488, 702
Romanowsky A. J., Douglas N. G., Arnaboldi M., Kuijken K., Merrifield M. R., Napolitano N. R., Capaccioli M., Freeman K. C., 2003, Sci, 301, 1696
Rusin D., Kochanek C. S., 2005, ApJ, 623, 666
Rusin D., Ma C., 2001, ApJ, 549, L33
Saglia R. P., Bertin G., Stiavelli M., 1992, ApJ, 384, 433
Sánchez-Blázquez P. et al., 2006, MNRAS, 371, 703
Seljak U., 2002, MNRAS, 334, 797
Thomas J., Saglia R. P., Bender R., Thomas D., Gebhardt K., Magorrian J., Corsini E. M., Wegner G., 2007, MNRAS, 382, 657
Tortora C., Napolitano N. R., Romanowsky A. J., Capaccioli M., Covone G., 2009, MNRAS, 396, 1132
Trager S. C., Faber S. M., Worthey G., González J. J., 2000a, AJ, 119, 1645
Trager S. C., Faber S. M., Worthey G., González J. J., 2000b, AJ, 120, 165
Treu T., 2010, ARA&A, 48, 87
Treu T., Koopmans L. V. E., 2002, ApJ, 575, 87
Treu T., Koopmans L. V. E., 2003, American Astron. Soc. Meeting, 203, 6801
Treu T., Koopmans L. V. E., 2004, ApJ, 611, 739
Treu T., Koopmans L. V. E., Bolton A. S., Burles S., Moustakas L. A., 2006, ApJ, 650, 1219
Treu T., Gavazzi R., Gorecki A., Marshall P. J., Koopmans L. V. E., Bolton A. S., Moustakas L. A., Burles S., 2009, ApJ, 690, 670
Treu T., Auger M. W., Koopmans L. V. E., Gavazzi R., Marshall P. J., Bolton A. S., 2010, ApJ, 709, 1202
van der Marel R. P., Franx M., 1993, ApJ, 407, 525
van Dokkum P. G., 2001, PASP, 113, 1420
van Dokkum P., 2008, ApJ, 674, 29
van Dokkum P., Conroy C., 2010, Nat, 468, 7326
Weijmans A.-M., Krajnovic D., van de Ven G., Oosterloo T. A., Morganti R., de Zeeuw P. T., 2008, MNRAS, 383, 1343
White S. D. M., Rees M., 1978, MNRAS, 183, 341
Worthey G., Faber S. M., Gonzalez J. J., 1992, ApJ, 398, 69
Wucknitz O., 2002, MNRAS, 332, 951
Zaritsky D., Gonzalez A. H., Zabludoff A. I., 2006, ApJ, 638, 725

This paper has been typeset from a TEX/LATEX file prepared by the author.